Journal of The Electrochemical Society, **163** (9) D506-D514 (2016)
0013-4651/2016/163(9)/D506/9/$33.00

Electrodeposition of Photoactive Silicon Films for Low-Cost Solar Cells

Ji Zhao,[=] Huayi Yin,[=] Taeho Lim, Hongwei Xie, Hsien-Yi Hsu, Fardad Forouzan,[a] and Allen J. Bard[*,z]

Center for Electrochemistry, Department of Chemistry, The University of Texas at Austin, Austin, Texas 78712, USA

Here we demonstrate progress on electrodeposition of photoactive silicon films from an environmentally friendly molten $CaCl_2$ electrolyte, which is the first step of a new route to a practical low-cost silicon solar cell. We report electrodeposition of several-micron thick silicon films on a graphite substrate in a bath of molten $CaCl_2$ containing SiO_2 nanoparticles. The best silicon deposits was obtained at 6 mA/cm^2 for 1 hour in molten $CaCl_2$ containing 0.3 M SiO_2 nanoparticles, at 850°C. The main impurities are Al, Mg, Ca, Na. A photoelectrochemical method was demonstrated as a reliable and sensitive measurement for testing the quality of the silicon film. The as-deposited film exhibits 31% of the photocurrent response of a commercial *p*-type wafer. A comparison of graphite and silver substrates is presented, and the remaining problems are discussed.
 [DOI: 10.1149/2.0731609jes]

Manuscript submitted April 4, 2016; revised manuscript received June 27, 2016. Published July 15, 2016.

We describe the state-of-the-art electrodeposition of Si films for use in solid-state photovoltaics, and methods of their characterization. We also discuss the remaining problems that must be solved before practical photovoltaic cells can be produced. Crystalline silicon photovoltaic cells (single crystalline and multicrystalline) are the dominant solar cells in the past 30 years, comprising over 90% in year 2014, and the trend will likely continue for the foreseeable future.[1] Although the commercial use of solar cells has been increasing (accumulated to 230 GW in 2015), the levelized cost of the electricity from crystalline silicon solar cells is still much higher than that from fossil fuels, which limits their competitiveness.[2] The United States has established goals for the year 2020 of $0.50/W for the solar cell module, $1.00/W for the solar cell system cost, and approximately $0.05/kWh for the levelized cost of solar electricity.[3] And to approach this goal, to reduce the cost from silicon material is critical. Since the photovoltaic module price consists of four parts: silicon material, wafer cutting, cell processing and module conversion.[4] And silicon is still the biggest part of the cost, due to the intensive equipment investment, high energy consumption in purification and material loss due to wafer cutting.[5]

Recently, research has focused on thin-film crystalline silicon solar cells to decrease the Si cost per peak watt.[6–8] Thin-film crystalline silicon solar cells not only reduce the amount of silicon used, but also promise low-cost processing and lightweight mechanical flexibility for modules. With effective anti-reflection and light trapping, 10% and 13.7% power conversion efficiency results have been achieved on the ~2 μm and ~10 μm thick crystalline silicon solar cell respectively.[6,7] Another advantage of thin-film silicon is that the minority carrier lifetime can be much lower than that of a bulk crystalline silicon solar cell. Theoretically, a 10 μm thick solar cell with a 10 μs minority carrier lifetime can still reach an efficiency close to 20%, compared with more than 1 ms needed for reaching same efficiency for a solar cell >150 μm thick. Because of the higher density of the carriers, the open circuit voltage of the cell can remain the same or be even higher.[7] Thus, a thin-film crystalline silicon solar cell has a higher tolerance to impurities, which allows the use of less-pure, lower-cost silicon. According to recent research results and theoretical analysis, preparing a silicon solar cell by electrodepositing a silicon layer directly on a substrate is a promising lower-cost substitute for the Siemens process and wafer cutting.

Electrolytic methods are among the most inexpensive ways to produce metals (Al, Ca, Mg, Na, K, etc.) or to prepare films on substrates.[9] Inspired by aluminum electrowinning from molten salts, researchers have studied electrolysis to prepare silicon.[10,11] Several different molten salt systems have been investigated and the review of the research can be seen in our previous work and other review papers.[12,13] Considering to prepare silicon device directly instead of only silicon material, the most significant result is from Rao in 1981, in molten LiF-KF at 745°C, with a reported purity of a silicon layer up to 99.995%. However, no further studies of this system have emerged.[14] During the ensuing years, interest has focused on molten $CaCl_2$ at about 850°C, in which oxides like TiO_2 can be reduced (deoxidization). When used for the electrolysis of SiO_2, the current efficiency can be above 86% and the electrolysis energy consumption can be as low as 10 kWh/kg Si, which is much lower than the polycrystalline silicon from the Siemens Process (above 80 kWh/kg Si).[15,16] However, the silicon prepared from the method above is still unsuitable for direct use in solar cells, because the morphology is mainly a powdered structure or nanowires, and normally with high impurity levels.[17–19] Recently researchers from Japan reported a film-like silicon deposit on silver from KF-KCl molten salt with $K2SiF_6$ as silicon feedstock. However, there is no proof of photoactive property on this silicon layer.[20,21]

The first photoactive crystalline silicon by electrodeposition was demonstrated on a silver substrate using a SiO_2 nanoparticle feedstock in a $CaCl_2$ melt.[12] Although the preliminary result revealed a photocurrent much lower than that of a commercial wafer, this result demonstrated the potential ability to use an electrodeposited silicon thin film for solar cells. The goal is to produce a dense, coherent, *p*-type silicon film with good quality (photoelectrochemical response) by electrodeposition on a proper substrate. The further vision is to prepare similarly a *p-n* junction and metal grid contact on top to provide a proof-of-concept solar cell device prepared by a new low-cost processing route.

In this paper, we report graphite as a substrate for electrodepositing silicon film from molten $CaCl_2$ with SiO_2 nanoparticles as the silicon feedstock. Graphite and silver substrates for silicon deposition are compared, and the remaining problems toward a solid-state silicon photovoltaic cell are discussed. Additionally, we report on a convenient photoelectrochemical technique for testing the quality of as-deposited silicon by means of a semiconductor-liquid-junction photoelectrochemical cell.

Experimental

Electrodeposition.—As shown in Figure 1, the molten salt vessel is an assembly comprised of a one-end-sealed quartz-flanged tube (o.d. 52 mm, length 500 mm) with an O-ring and a stainless steel lid, a one-end-sealed lining quartz tube (o.d. 45 mm, length 300 mm), and an alumina crucible (i.d. 33 mm, length 95 mm, 99.95%, Ad-Value Technology, Tucson, AZ). The flange lid has O-ring structured holes through which the conducting wires with electrodes are inserted. $CaCl_2 \cdot 2H_2O$ (calcium chloride dihydrate, ACS, 99 to 105%,

[=]These authors contributed equally to this work.
*Electrochemical Society Fellow.
[a]Present address: ARTIN Engineering and Consulting Group, Inc. San Diego, California, USA.
[z]E-mail: ajbard@cm.utexas.edu

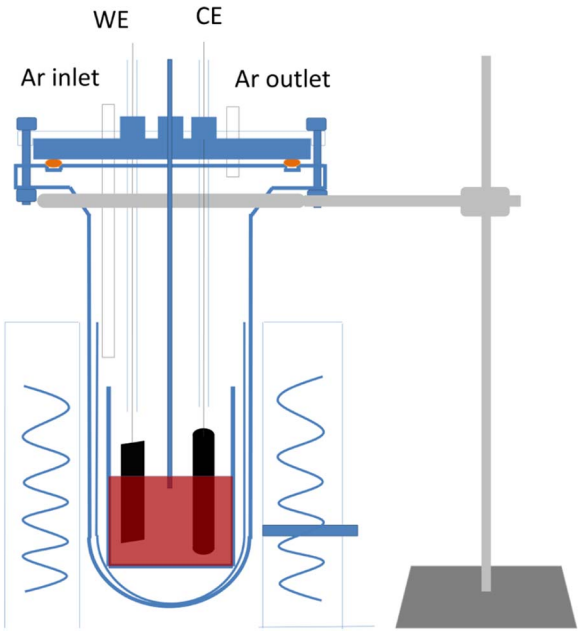

Figure 1. Schematic drawing of the set up for the molten salt electrodeposition.

Alfa Aesar, Haverhill, MA) was baked at 180°C in a vacuum oven for a minimum of 12 hours before use.

In a typical experiment, 0.5 g SiO_2 nanoparticles (silicon dioxide, 10–20 nm particle size, 99.5%, Aldrich, St. Louis, MO) and 50 g $CaCl_2$ was weighed and poured into a narrow-mouth bottle and then mixed using a blender at 2000 rpm for 2 min. After mixing, the mixture was poured into the dry alumina crucible and then placed into the lining tube and finally the quartz-flanged tube. The lid was affixed and the entire vessel was sealed. The bottom part of the vessel was heated in a tube furnace (Model F21135, 1350 W, Thermo Scientific, Waltham, MA) in a vacuum for 2 hours at 400°C to remove moisture. With argon gas (99.95%) purging into the vessel, the furnace was heated to 850°C and the electrodeposition conducted. The salt bath was approximately 30 mm in depth and the temperature difference within that region was less than 10°C. The working electrode (cathode) was a graphite strip from one of several different graphite sources: a) premium graphite (POCO AXF-5Q, Entegris POCO, Decatur, TX) cut to 75 × 6 × 1 mm, b) McMaster graphite (premium grade, McMaster Carr, Elmhurst, IL), cut to 75 × 6 × 1 mm, or c) carbon foil, (0.5 mm thickness, 99.8%, Aldrich, St. Louis, MO) cut to 75 × 7 mm. Solid graphites a) and b) were polished by sandpapers (600 and 1200 grit MicroCut Discs, Buehler, Lake Bluff, IL) to a mirror finish. The counter electrode was a graphite rod (0.25" graphite rod, 99.995%, Alfa Aesar, Haverhill, MA). The rod was cut to a length of 75 mm and immersed into the salt bath at 25 mm. The electrode leads were tungsten wires (d. 1 mm, length 600 mm), each sealed in a quartz tube by epoxy on top. A graphite connector made from a graphite rod was used to connect the tungsten wire and electrode, with molybdenum wire (d. 0.25 mm) bind the graphite electrode onto the graphite connector.

The cathode was immersed about 20 mm into the bath and electrodeposition experiments were carried out at a constant current using an Autolab PGSTAT 128N potentiostat/galvanostat (Metrohm, Utrecht, NL). The electrodeposition was carried out in constant current way with the current density in the range of 2 to 8 mA/cm^2. After the deposition, the cathode was removed slowly and held in the vessel above the bath in an argon atmosphere to cool down. Then the sample was taken out from the vessel, thoroughly rinsed with water followed by ethanol, and dried in an oven at 120°C.

Photoelectrochemical (PEC) characterization of the deposit.— Electrodeposited Si films on graphite or silver substrates were cut into 6 mm × 6 mm squares to prepare working electrodes for PEC measurement. A Si deposit on one edge of a substrate was then removed by mild polishing to provide an area for electrical contact made by connecting a Cu wire to the polished side with Cu tape. The exposed geometric area of the Si film was defined at about 0.24 cm^2 by applying chemically inert epoxy (Loctite 1C-LV, Hysol) to insulate the rest of the electrode. Epoxy-covered electrodes were then dried overnight in air.

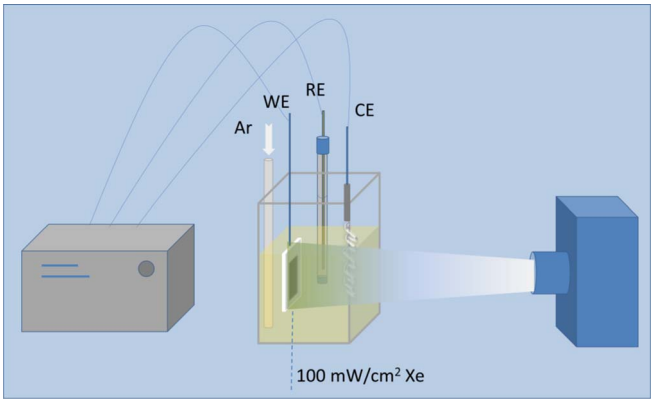

Figure 2. Schematic drawing of the photoelectrochemical (PEC) cell test for a silicon film or wafer.

PEC measurements were carried out in a 1-mm-thick quartz glass cell (W: 25.4 mm, L: 25.4 mm, H: 50 mm) using a three-electrode configuration with a Pt-wire counter electrode and non-aqueous $Ag/AgNO_3$ (0.01 M in MeCN) reference electrode (MF-2062, BAS) (Figure 2). The electrolyte was Ar-purged MeCN (CH_3CN, 99.9%, Extra Dry, Acros, Fair Lawn, NJ) containing 0.1 M tetrabutylammonium hexafluorophosphate ($TBAPF_6$, ≥99.9%, Fluka, Allentown, PA) as supporting electrolyte and 0.05 M ethyl viologen diperchlorate ($EV(ClO_4)_2$, 98%, Sigma-Aldrich, St. Louis, MO) as a redox agent. The potential and current of Si films were measured with a scan rate of 10 mV/s under UV-visible light irradiation using a CHI 760E potentiostat (CH Instruments, Austin, TX). The working electrode under test was irradiated through the electrolyte by using a Xe lamp (Oriel, 150 W) with light intensity of 100 mW/cm^2 at the electrode surface, assuming negligible electrolyte absorption. A single crystalline Si wafer (5–10 ohm · cm, (100), boron-doped, University Wafers, Boston, MA) was used as a standard working electrode. Ohmic contact to the Si wafer was made by thermal evaporation of Au (30 nm) on the back. The rest of the working electrode preparation, for example masking with epoxy, was the same as above. To remove native silicon oxides before electrochemical measurements, all Si electrodes were immersed in a 5 M hydrofluoric acid solution (HF, 48–51% in water, Acros, Fair Lawn, NJ) for 5 min, and then rinsed with deionized water and then MeCN.

Materials characterization.— Silicon films were characterized by scanning electron microscopy (SEM, Quanta 650 FEG, FEI Company, Inc., Hillsboro, OR) equipped for energy dispersive spectroscopy (EDS, XFlash Detector 5010, Bruker, Fitchburg, WI), and time-of-flight secondary-ion mass spectroscopy (TOF-SIMS, Perkin-Elmer, Model ULVAC-PHI TFS2000 system equipped with a Bi-ion source), X-ray photoelectron spectroscopy (Kratos XPS, Kratos Analytical Ltd., UK) equipped with a monochromatic Al X-ray source, and X-ray diffraction spectroscopy (XRD, Philips X-ray diffractometer equipped with Cu Kα radiation).

Results and Discussion

Photoelectrochemical cell test methodology for semiconductor film.— Rather than fabricating a *p-n* junction to test these films in a solid-state photovoltaic (PV) cell, a simpler way to characterize

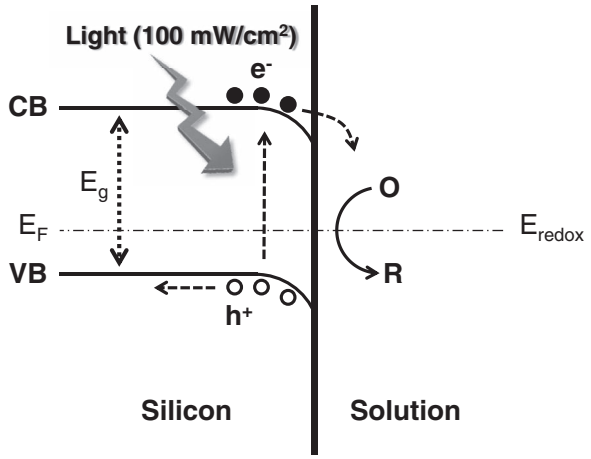

Figure 3. Schematic diagram of *p*-type Si/liquid junction with redox agent, where CB and VB stand for conduction band and valence band, E_F and E_g are Fermi level and bandgap of Si, E_{redox} is standard reduction potential of redox agent.

photoactive semiconductor materials is to assemble a photoelectrochemical (PEC) cell by making a semiconductor/liquid junction with the film to be tested and adding a counter electrode. In this way, technical problems can be avoided arising from interface contact or from multiple variable parameters in full device architecture and solid-state fabrication. In contrast, the semiconductor/liquid junction in a PEC cell is relatively reliable (if proper liquid electrolyte is employed) and the PEC cell structure is very simple and easy to realize in a chemistry lab. We have previously demonstrated that performance of $CuInSe_2$ and $Cu(In_{1-x}Ga_x)Se_2$ thin films in a PEC cell corresponds well to their observed performance in a full solid-state PV cell.[22] Here an effective PEC cell system for *p*-type Si was employed as reported previously.[12]

Figure 3 shows an ideal model of a semiconductor/liquid junction for a *p*-type Si electrode with redox reagents. Photoelectrochemical reduction of redox reagent occurs when the electrode is irradiated by light having enough energy to excite electrons through the bandgap (E_g), producing a photocurrent. Electrons in the conduction band (CB) that are consumed to reduce the redox agent determine the amount of photocurrent; these electrons are continuously transferred from the back contact. Some electrons are not utilized in the reduction process because of energy loss mechanisms, such as electron-hole recombination. In the absence of light, no photocurrent flows, as there are no electrons available for photoelectrochemical reduction in the conduction band. However, if there are pinholes exposing a conductive substrate or impurities in the semiconductor electrode, a general electrochemical reduction reaction may take place even without light. This electrochemical current is called dark current and qualitatively indicates the extent to which defect sites are present at the semiconductor electrode surface.

In this study, we chose ethyl viologen (EV^{2+}) as a redox reagent in acetonitrile (MeCN) solvent because the redox reaction of $EV^{2+/+}$ is a reversible, single-electron, outer-sphere reaction that is independent of electrode material, while its standard reduction potential is within the Si bandgap.[23,24] The light absorbance of EV^{2+} is also relatively low compared to other available redox chemicals. The redox reactions of $EV^{2+/+}$ and $EV^{+/0}$ on a Au disk electrode (d. 25 μm) in MeCN are shown in Figure 4a. Two reversible redox reactions were clearly observed with half-wave potentials ($E_{1/2}$) of −0.75 V and −1.16 V vs $Ag/AgNO_3$ for the first and second reduction steps, respectively. These correlate with previously reported values, −0.48 V and −0.89 V vs Ag/AgCl (saturated KCl).[25] The potential of $Ag/AgNO_3$ (0.01 M in MeCN) is about 0.34 V vs Ag/AgCl (saturated KCl) in aqueous media. Figure 4b shows photoelectrochemical behavior of a *p*-type Si wafer electrode (5–10 ohm · cm, (100), boron-doped, University Wafers, Boston, MA) in the system. A photocurrent due to photoelectrochemical reduction of EV^{2+} was obtained when light was illuminated while no photocurrent was measured in the dark.

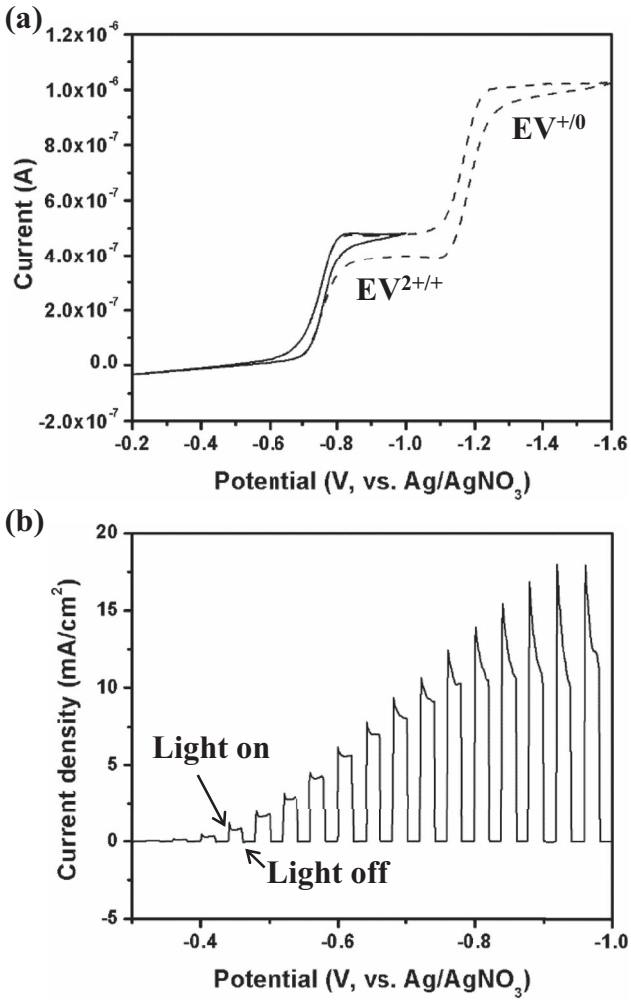

Figure 4. (a) Current-potential curve of an Au disk electrode (d. 25 μm), $EV^{2+} \leftrightarrow EV^{+}$ (solid line) and $EV^{2+} \leftrightarrow EV^{+} \leftrightarrow EV^{0}$ (dashed line). The scan rate was 500 mV/s. (b) Current-potential curve of a *p*-type Si wafer electrode under 100 mW/cm² of illumination with a scan rate of 10 mV/s. The light was chopped at 2 s intervals. Both curves were obtained in Ar-purged MeCN containing 0.1 M $TABAF_6$ and 0.05 M $EV(ClO_4)_2$.

The short-circuit current density (J_{sc}) at −0.75 V vs $Ag/AgNO_3$ was about 10 mA/cm². The ideal maximum photocurrent density under illumination of 100 mW/cm² (AM 1.5G) for *p*-type Si is 44 mA/cm² based on the conventional Shockley-Quisser limit for solar cell energy conversion.[26] Our Si wafer electrode didn't meet the maximum photocurrent because the strong blue color of reduced EV^{+} blocked the portion of light at the electrode surface during the measurement, especially at the more negative potential region than −0.8 V vs. Ag/AgNO3. Other factors, such as non-radiative recombination of photo-generated charge carriers, light reflection, or charge transfer resistance from semiconductor to redox agent, may also degrade the photocurrent. About 9.3 mA/cm² of short-circuit current density (J_{sc}) was previously reported with EV^{2+} at *p*-type Si (3 ohm · cm, under 100 mW/cm²) by our group.[27] Some investigations were performed with methyl viologen (MV^{2+}), which has a similar standard reduction potential to that of EV^{2+}.[28] Typical J_{sc} of MV^{2+} reduction in aqueous media has been reported as 20 (±3) mA/cm² on *p*-type Si (0.6–0.8 ohm · cm) under 60 mW/cm² of 808 nm illumination, producing a photon flux above the Si bandgap analogous to that obtained from broadband illumination (100 mW/cm², AM 1.5).[29]

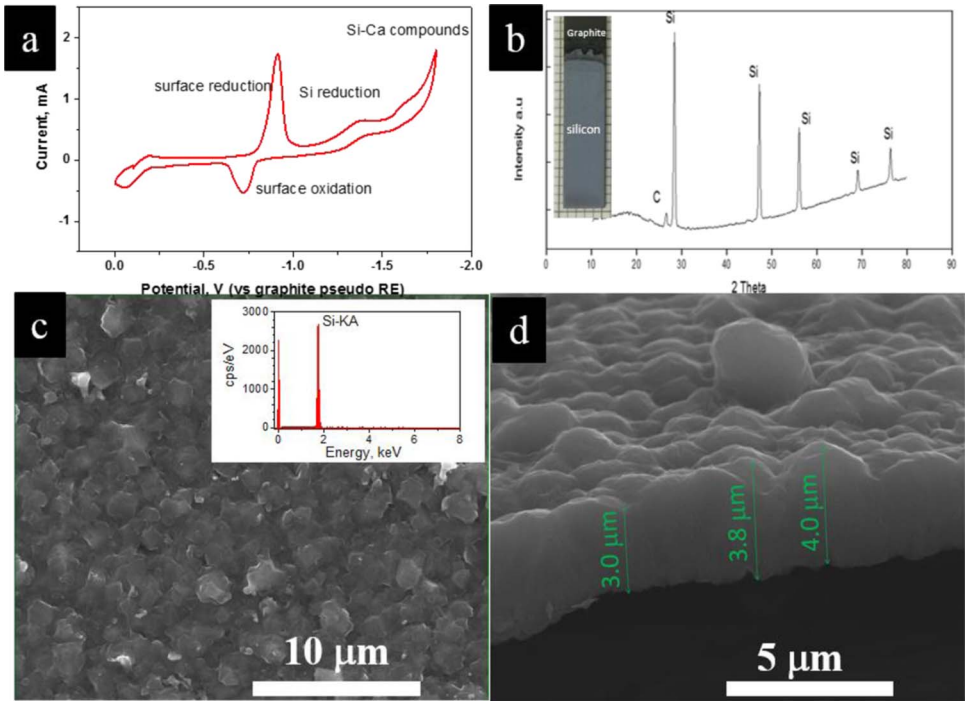

Figure 5. (a) Cyclic voltammetry of graphite (d. 3 mm × length 2 mm) at 850°C in $CaCl_2$ containing 0.3 M SiO_2 nanoparticles. (b) XRD patterns of the as prepared silicon film on graphite, with inset digital picture of the deposit. (c) Typical top view SEM image of the deposit silicon on graphite, with inset EDX spectrum. (d) Cross sectional SEM image on a film peeled off from the graphite substrate.

The photoelectrochemical behavior of electrodeposited Si on silver and graphite was measured similarly, with the following caveat. Because $E_{1/2}$ for the $EV^{2+/+}$ reaction was measured at −0.75 V vs $Ag/AgNO_3$ (0.01 M in MeCN) in MeCN, J_{sc} for the electrodeposited Si film can be considered to be the photocurrent density at −0.75 V. However, a significant amount of dark current from the electrodeposited Si film at −0.75 V, due to pinholes in the deposit, disturbed the accurate measurement of J_{sc}.[30] The effect of the color change by the reduction of EV^{2+} to EV^{+} was also negligible at this potential. For quantitative comparison with a standard *p*-type Si wafer electrode, the photocurrent density value was measured at −0.62 V where the dark current was negligible.

Graphite substrate.—Here we report that a graphite substrate can be used for electrodeposition of a silicon film using SiO_2 nanoparticles as silicon feedstock in molten $CaCl_2$. Although graphite has been reported as substrate for silicon deposition in molten fluoride,[14,31] to the best of our knowledge, this is the first time that graphite has been proved as a substrate for electrodepositing a photoactive dense silicon film in molten chloride bath.

A typical cyclic voltammogram for reduction of SiO_2 nanoparticles on graphite in $CaCl_2$ bath is shown in Figure 5a. The reduction on graphite is similar to the process on silver, where the reduction curve starts at −1.1 V versus a graphite pseudo-reference electrode. A typical silicon film on graphite appears uniform with a light blue-gray color (Figure 5b inset), and XRD patterns (Figure 5b) show that the film is polycrystalline with no preference in crystalline direction. A top-view SEM image (Figure 5c) shows a film composed of crystalline grains of several microns in size and well covered, with low impurities as measured by EDX (Figure 5c inset). From one cross-sectional SEM image (Figure 5d), the dense film produced by deposition at 6 mA/cm^2 for 1 h is approximately 3–4 µm thick with around 4-µm surface roughness.

At 6 mA/cm^2, a silicon film was formed within 2 minutes, as shown in Figure 6a. As the deposition time extended to more than 1 hour at 6 mA/cm^2, the surface became rougher and a primarily dendritic structure emerged on top of a dense layer (Figure 6b). From XPS data, it was clear that the dense layer was elemental silicon. Additionally, a silicon carbide layer was identified at the interface of graphite substrate and the silicon film, as shown in XPS data in Figure 6c and in the SiC signal in the SIMS data in Figure 6d. At 850°C, the formation of SiC from Si and C is thermodynamically spontaneous ($Si + C \rightleftharpoons SiC$, $\Delta G = -62.8$ kJ). So the initial SiO_2 reduction on graphite is possibly a combination of electrodeposition and chemical reaction. Our previous results show that although silicon can be reduced from SiO_2 nanoparticles, it is difficult to grow a dense silicon film with reasonable thickness on metals substrate like Mo.[32] This SiC interface layer may help to buffer the stress between the silicon film and graphite substrate and assist in forming a coherent dense film of silicon. SIMS profile analysis reveals that impurities distribute mainly on the interface of the graphite substrate and the silicon film (that is, in the same range with the SiC interlayer) and on the top surface of silicon. The major impurities are Ca, Al, Mg, Mn. These impurities could come from salt (Ca, Mg), the stainless steel cap(Mn), and the Alumina crucible and SiO_2 feedstock (Al, Mg). As discussed further below, the silicon films prepared in this series of experiments are all *p*-type as deposited. Al and Mg impurities, combined with the existence of B, may explain this *p*-type behavior.[33]

The quality of silicon coverage and the PEC response varied with different types of graphite substrates. As depicted in Figures 7b–7d, three kinds of graphite substrates have been tested: soft carbon foil (0.5 mm thick), normal rigid graphite (from McMaster Carr), and premium graphite (POCO Graphite, AXF-5Q, with finer micro structure and better uniformity). The detailed properties of these substrates are listed in Table I. Generally, graphite foil is a type of soft graphite material composed of compressed exfoliated graphite flakes with a layer-stacked structure and a surface composed of flat graphite flakes. The mechanical strength of carbon foil is too weak to keep its macroscopic shape during heating and cooling. As a result, the film grown on it can be easily cracked (Figure 7e), which leads to a significant dark current in the PEC test. As portrayed in Figure 7g, the dark current of a silicon film is higher on graphite foil than on premium graphite (POCO Graphite AXF-5Q), although the photocurrents are similar.

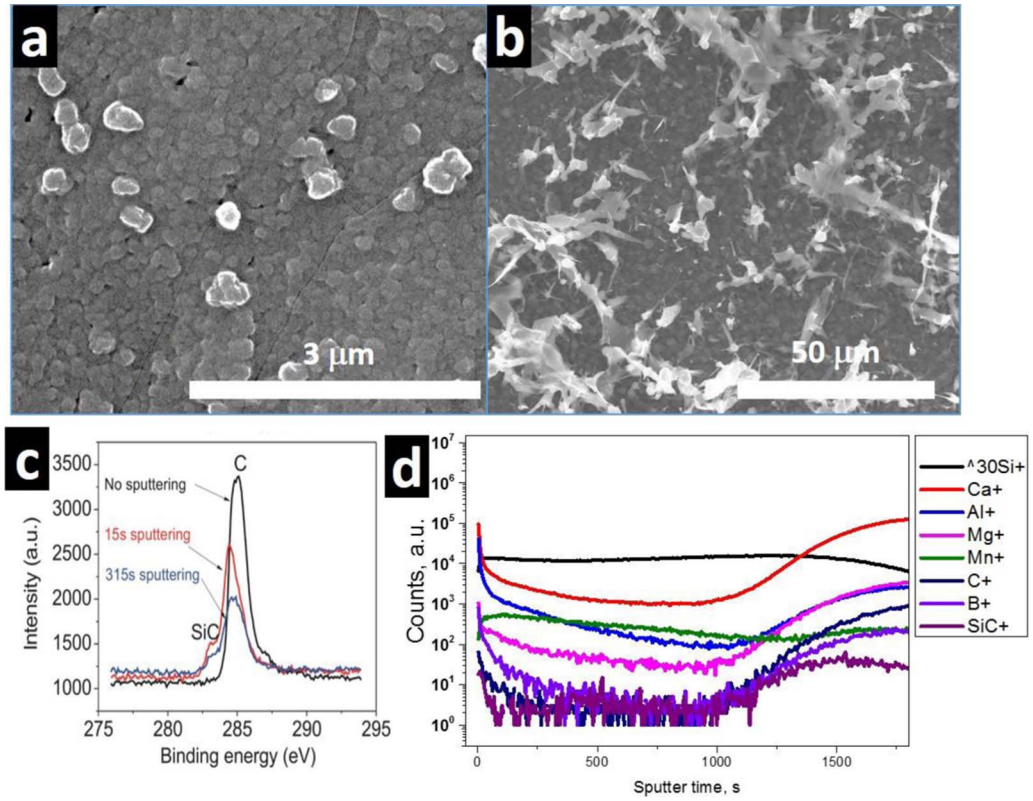

Figure 6. (a) (b) SEM images of silicon film deposited at 6 mA/cm^2 for 2 min and 3 h, respectively. (c) XPS spectra of the C peak for the 2 min deposited sample with sputtering time indicated. (d) SIMS profile spectra of sample deposited at 6 mA/cm^2 for 1 h.

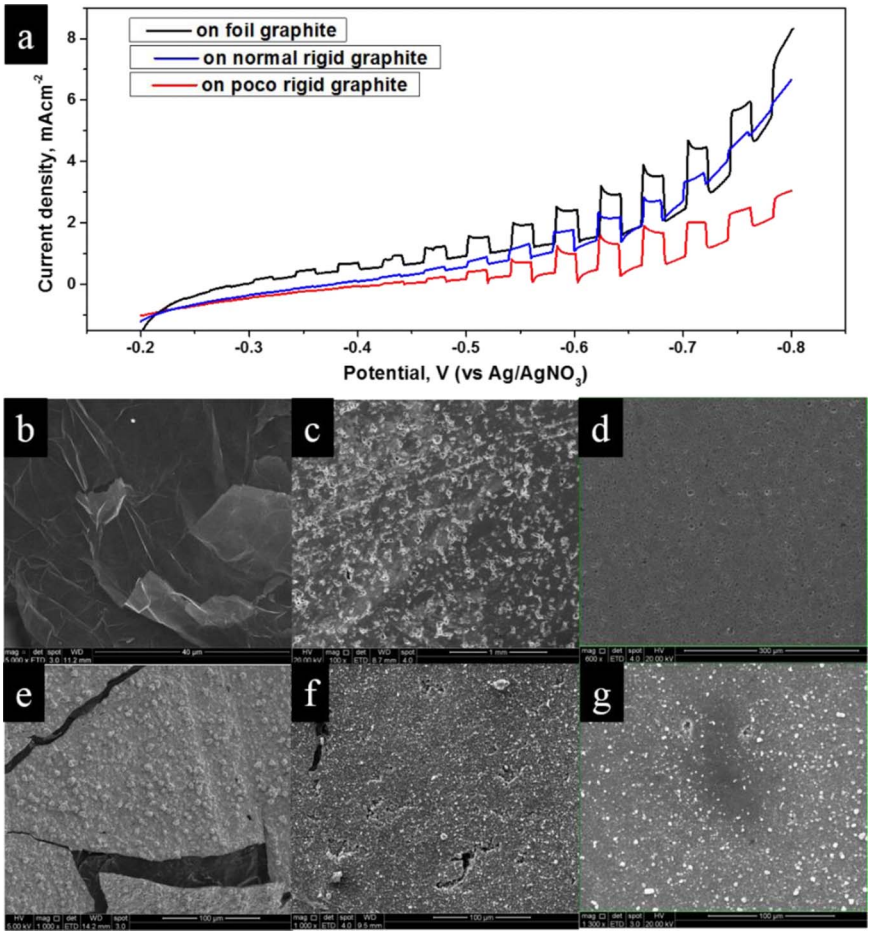

Figure 7. (a) PEC plots of the silicon film deposited on graphite foil, normal graphite and POCO graphite. (b–d) SEM images of substrates: foil (b), normal (c), and POCO graphite (d). (e–g) SEM images of silicon deposits on foil (e), normal (f) and POCO graphite (g).

Table I. Properties of different graphite substrates.

Property	Graphite Foil	Normal graphite	Premium Graphite (POCO AXF-5Q)
Particle size, μm		10	5
Pore size, μm		5	0.8
Apparent density, g/cm^3	1.0	1.82	1.78
Compressive strength, MPa	200	127	138
Electrical resistivity, μΩ · cm		1400	1470
Ash content, ppm	5000	5000	500

In contrast to the graphite foil, rigid graphite strips (of either normal graphite and POCO graphite, 1.0 mm thick) are robust enough to avoid cracking during temperature changes. The thermal expansion coefficients are similar (volumetric coefficient of thermal expansion, $\alpha_{V,\mathrm{Si}} = 4.68 \times 10^{-6}$ K^{-1}, and $\alpha_{V,\mathrm{graphite}} = 6.5 \times 10^{-6}$ K^{-1}),[34] hence thermal stresses between the deposit and substrate should be tolerable. As shown in Figures 7f–7g, no cracks can be seen in the deposits from these substrates.

However, as shown in Table I, macro pores exist on the surface of some graphite materials. Normal graphite (5 μm average pore size) contains some macro pores that are larger than the thickness of the silicon film; those places are poorly covered by silicon, leaving an exposed graphite substrate and causing dark current in the PEC test. Premium graphite (POCO graphite AXF-5Q, 0.8 μm average pore size) has far fewer macro pores on its surface (although still not zero). As a result, the dark current from silicon films is generally less on POCO graphite than on normal graphite. This effect is apparent in Figure 7a, where the silicon film deposited on normal graphite reveals a high dark current similar to the sample on graphite foil, due to the large area of the defects on the substrate surface. Premium graphite gives the smallest dark current and almost the same (the highest) photocurrent among the three kinds of graphite substrates. For the purpose of preparing dense, pinhole-free silicon films for application in photovoltaic devices, premium graphite (POCO Graphite AXF-5Q) was chosen as the substrate for further experiments because of its low macro-pore density and consistent quality.

The morphology of electrodeposited silicon can be tuned by current density and the quality of the film can be measured by PEC analysis. As shown in Figures 8b–8e, as current density increased from 2 to 8 mA/cm^2, the grain size of the film became finer. A synergetic effect from nucleation and growth processes can explain the deposit morphology qualitatively. Lower current density creates a low density of nuclei, causing coarse grain growth and a film with low coverage; higher current density creates a high density of nuclei that is good for a dense film, but the growth process may be mass-transfer limited and diffusion control can result in dendritic morphology.[35] The optimum film with good density and coverage is expected to be deposited at a moderate current density.

Figure 8a shows the PEC results for four silicon films made at different current densities for different amounts of time, but the same overall charge (21.6 C/cm^2). The silicon film deposited at 6 mA/cm^2 for 1 h stands out as having both lowest dark current (indicating best coverage of the film) and highest photocurrents (indicating good crystalline structure and good adhesion to substrate). Samples deposited at 4 mA/cm^2 for 1.5 h shows almost the same photocurrent as the sample of 6 mA/cm^2, but a higher dark current, which is indicative that the crystalline quality of the film is good but the coverage is not as good as 6-mA/cm^2 sample. In the SEM image, one can see the similar grain size film morphology between 4-mA/cm^2 1.5-h samples and 6-mA/cm^2 1-h sample (Figures 8c–8d), although coverage is less uniform. Interestingly, for the 2-mA/cm^2 sample, PEC not only reveals the highest dark current among samples in the series, owning to a large number of pinholes among a coarse grain; but also reveals a tiny photocurrent response, which indicates that a bad connection between the silicon film and substrate, which cannot be observed by

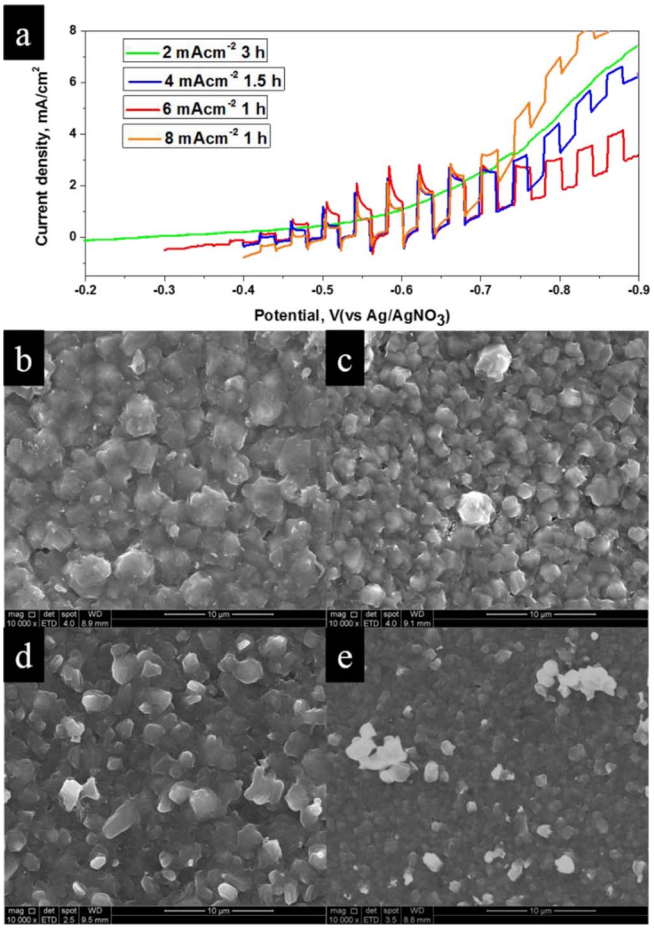

Figure 8. (a) PEC plots of silicon films prepared by electrodeposition at different current densities from 2 mA/cm^2 to 8 mA/cm^2, but the same overall charge (21.6 C/cm^2), in a $CaCl_2$ bath containing 0.3 M SiO_2 nanoparticles. (b–e): SEM images of the silicon film electrodeposited at (b) 2 mA/cm^2, (c) 4 mA/cm^2, (d) 6 mA/cm^2 and (e) 8 mA/cm^2.

SEM. For the 8-mA/cm^2 samples, the dark current is higher and the photocurrent is lower, compared with the 6-mA/cm^2 samples. The lower photocurrent has two possible reasons. First, the silicon film is thinner, because compared with the 6-mA/cm^2 the 1-h sample; the 8-mA/cm^2 0.75-h samples have more dendrites due to the effect of diffusion control from higher current density deposition. Secondly, at the higher current density the silicon film is composed of smaller grains and has more grain boundaries, which can provide recombination centers that impede transfer of charge carriers. The higher dark current can be from either more grain boundaries or pinholes due to the insufficient growth of the grains around dendrites.

Interestingly, increasing the deposition time in some cases does not improve the quality of the silicon film. As shown by the PEC test, the photocurrent only increases and the dark current slightly decreases. That is due to the current distribution that develops with dendrite structure growth. Since the dendrites are already developed in the one-hour deposition, extending the deposition time will primarily contribute more dendrite structures and not improve the dense film thickness or the exposed area. These dendrites are brownish in color showing poor connection to the dense silicon film; hence they contribute slightly to the PEC performance. The structure of the films on graphite was not a function of temperature between 800 and 900°C; the morphology, thickness, and roughness were essentially the same. Similarly a change in the concentration of silicon dioxide between 0.1 and 1.2 M didn't affect the structure. We believe that the SiO_2 nanoparticle plays a very important role as the feedstock in the deposition. Unlike larger pieces of SiO_2, it can be dispersed in the salt and

Table II. Best photocurrent densities of silicon films deposited on silver and graphite from SiO_2 nanoparticles in $CaCl_2$, with reference to standard wafer (*p*-type, 5–10 ohm · cm).

	Si film on silver	Si film on graphite	Wafer
Electrodeposition condition	5 mA/cm^2, 6 h, 820°C	6 mA/cm^2, 1 h, 850°C	—
Thickness, μm	7	3.5	500
Photocurrent @ −0.62 V vs Ag/$AgNO_3$, mA/cm^2	0.87	1.71	5.60
Photocurrent ratio	16%	31%	100%

result in a relatively uniform silicon feedstock in the salt bath. While at present the real state of silicon source has not been well established.

Overall, a coherent, dense, thin silicon film can be electrodeposited on graphite substrate. The optimum conditions observed for electrodeposition were 6 mA/cm^2 current density for 1 hour at 850°C in a molten $CaCl_2$ bath, with 0.3 M SiO_2 nanoparticles (Table II). The best photocurrent density observed for electrodeposited silicon on graphite at −0.62 V vs Ag/$AgNO_3$ was 1.71 mA/cm^2 (Figure 9a), which is 30% of the photoresponse of a silicon wafer. As shown in Figure 9b, the silicon film has poor photo harvest efficiency. The silicon film has a thickness of less than 4 μm, which is 45 times less than a wafer and light harvested is less than 55% (Figure 9b). We expect to achieve improved photoresponse from electrodeposited silicon films by improving the control over the level of impurities in the process.

Comparison graphite substrate with silver and discussion on electrodeposition silicon for solar cell.—Silver was the first substrate discovered for electrodeposition of photoactive silicon,[12] however, on silver the deposit is not a dense film. The appearance of the deposit (Figure 10a inset) is dark blue-black. From SEM observations, it

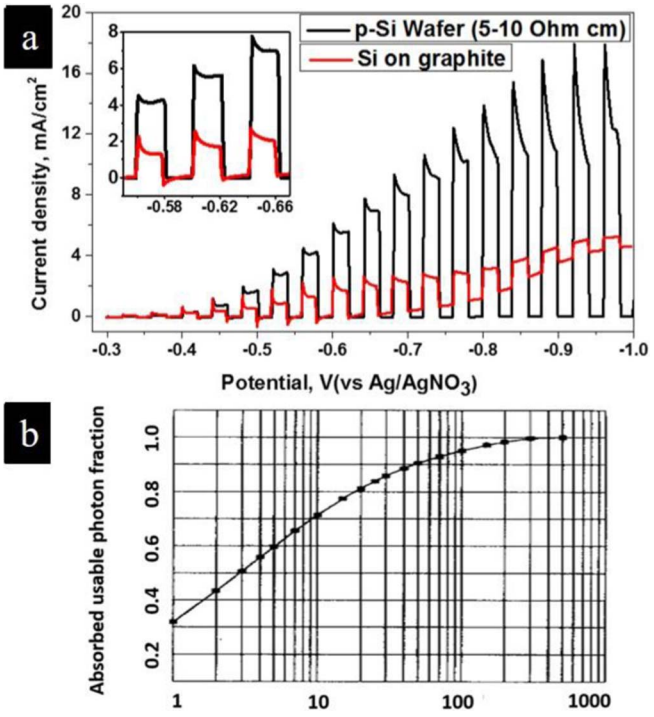

Figure 9. (a) The best reproducible current-potential performance curve of the electrodeposited Si film on graphite (6 mA/cm^2, 1 h) in Ar-purged MeCN containing 0.1 M $TABAF_6$ and 0.05 M $EV(ClO_4)_2$ under 100 mW/cm^2 of illumination, compared with a *p*-type silicon wafer (5–10 ohm · cm). The light was chopped at 2 s intervals. (b) The light adsorption of solar photon fraction as a function of silicon thickness for AM1.5 illumination.[34]

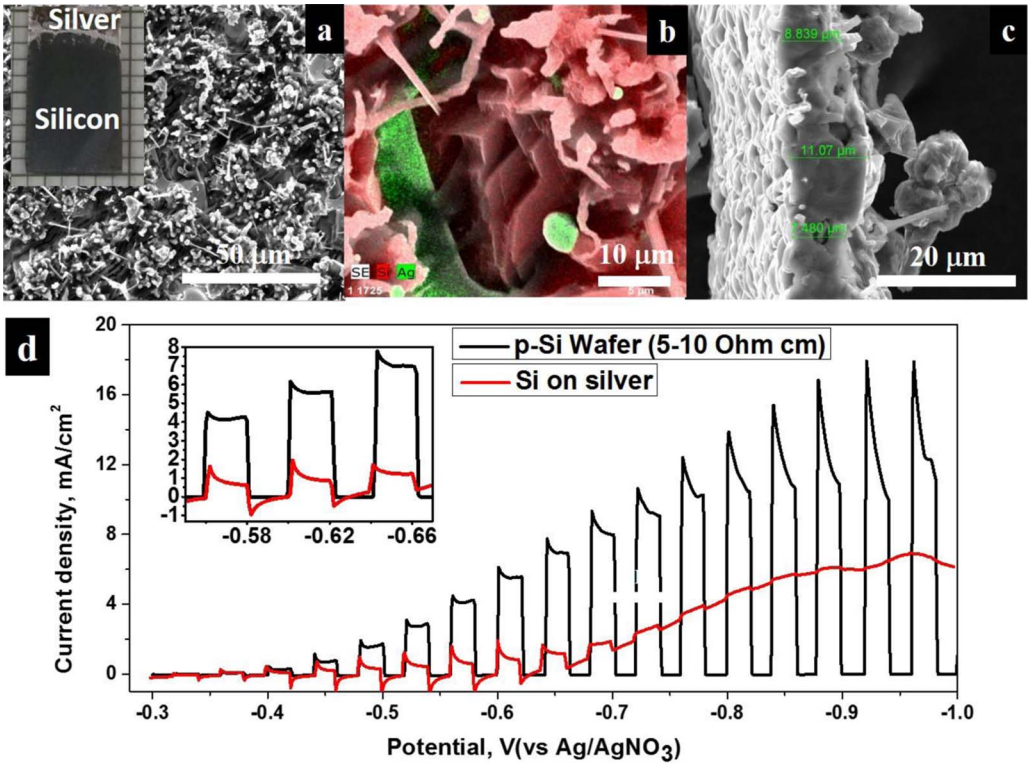

Figure 10. (a) One typical SEM top-view image of a silicon deposit on silver, with inset digital picture of the as-deposited silicon on silver sample. (b) EDX element mapping of the deposit in a higher magnification. (c) Cross-sectional view of the deposit break off from the substrate. (d) Best PEC result of silicon deposit on silver substrate (0.3M SiO_2 nanoparticles at 820°C in $CaCl_2$, 5 mA/cm^2, and 6 h), compared with a *p*-type wafer sample (5–10 ohm · cm).

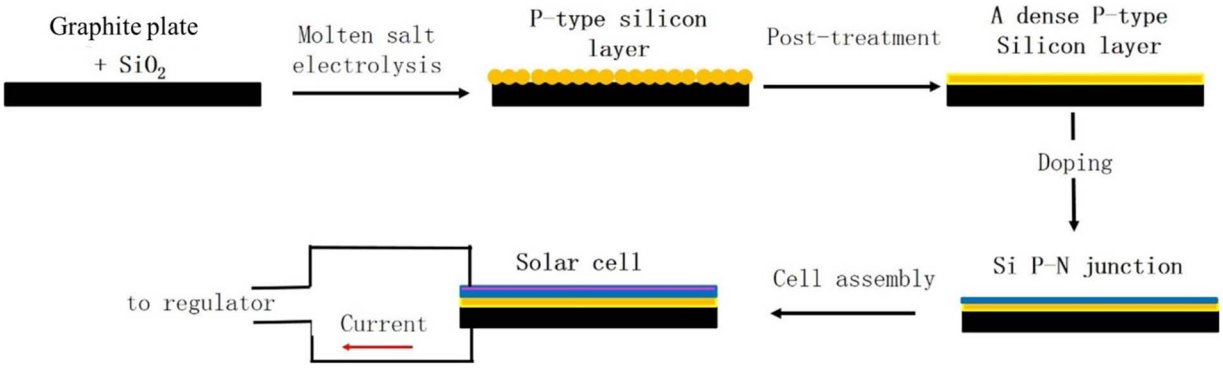

Figure 11. Flowchart of the strategy for producing a thin-film crystalline-silicon solar cell by molten-salt electrodeposition.

is actually composed of various sizes of clusters on top and denser deposits with exposed silver below (Figures 10a–10b). EDX mapping (Figure 10b) shows a slot-like exposed silver substrate on the top of the substrate surface. This exposed silver substrate will generate dark current in a PEC test, and will easily short circuit the device with no insulation covering it. The relatively denser deposit is approximately 7 μm in thickness with holes and tunnels within for a 6-h deposit sample (Figure 10c). Figure 10d shows the best photocurrent for silicon on silver. Overall, the photocurrent value from the best sample of silicon on a silver substrate was 0.87 mA/cm^2 at −0.62 V vs $Ag/AgNO_3$ reference, which is half of the value from the graphite substrate discussed previously, and only 15% of the photocurrent of a *p*-type silicon wafer (5–10 ohm · cm). The best condition for silicon growth on a silver substrate, based on the PEC response, is 5 mA/cm^2, 6 h of deposit at 820°C in $CaCl_2$ containing 0.3 M SiO_2 nanoparticles. The comparisons of the best deposit in terms of the PEC test result are listed in Table II. Generally, silicon on graphite has less deposition time (1 h vs 6 h), less thickness (3.5 μm vs 7.0 μm) but a higher photocurrent (1.71 mA/cm^2 vs 0.87 mA/cm^2) and smaller dark current, displaying a better quality and denser silicon deposit and is the more promising substrate for application in a solid-state solar cell.

The volumetric coefficient of thermal expansion for silver ($\alpha_{V,Ag}$ = 18.9 × 10^{-6} K^{-1}) and silicon ($\alpha_{V,Si}$ = 4.68 × 10^{-6} K^{-1}) are quite different, and this mismatch could explain the slot-like exposed silver substrate.[34] Considering that silicon is deposited above 800°C and must cool to room temperature before testing, the differential contraction of the two materials would have a strong influence on mechanical strength. While silver has good ductility and silicon is fragile with poor ductility, the silicon deposits may be easily crushed and peeled off by the contraction. The temperature for deposition on a silver substrate is preferably lower than 830°C, because above 830°C the silver substrate breaks at the surface of the molten salt bath.

We have already explained that the thin-film crystalline silicon solar cell is promising to be a new type of low-cost silicon solar cell. A strategy for low-cost production of a silicon solar cell by means of electrodeposition is described in Figure 11. We envision first using electrodeposition to prepare a *p*-type silicon layer, with possible post-treatment to improve the quality and morphology. Then, there would be an operation to dope the silicon to make a *p-n* junction, either by a conventional method or preferably by an additional molten-salt electrolysis step to make an *n*-type layer. Finally, the cell would be assembled with a front contact and packaging to prepare a thin-film crystalline silicon solar cell.

The key step now is the first step: to prepare a good quality *p*-type silicon film on a low-cost substrate. The objectives for this film are: a) purity higher than 99.999% to reduce the recombination; b) thickness near 10 μm to achieve good light harvesting without complicated light-trapping structures; c) a pinhole-free film with surface roughness less than 1 μm in order to go directly to the next processing step.

We believe that impurity control is a major problem to solve. This is because it is difficult to remove impurities from silicon films once the impurity has been reduced together with silicon, and also impurities will influence the growth of silicon. Once impurities can be controlled to a specific low level, the optimization of morphology can be conducted by various electrochemical methods. The substrate is also critical in the growth control of the silicon film. The solution requires a comprehensive deep understanding of high-temperature electrochemistry.

Conclusions

Electrodeposition of photoactive silicon films can be a promising first step to pave the road to low-cost thin-film crystalline-silicon solar cells. In this paper, the photoelectrochemical (PEC) cell method has been systematically illustrated for fast and convenient testing of the quality of an as-deposited silicon film. The PEC method can identify pinholes or any exposed substrate by dark current, the quality of the semiconductor film by photocurrent, and can provide a simple comparison of results with a standard silicon wafer.

Graphite was discovered as a good substrate for electrodeposition of a photoactive dense silicon film from a chloride molten salt. The deposit on graphite was generally a dense film of several-micron thick, with a SiC interface between the graphite substrate and silicon film. Among different kinds of graphite substrates, the silicon film obtained on the POCO graphite showed the best performance in terms of the dark current, which was due to a lower density of the macro pores on the graphite surface. The current density of the electrolysis governed the grain size and coverage of the silicon film, and the best condition observed, in terms of PEC response, was 6 mA/cm^2, 1 h, in a $CaCl_2$ melt containing 0.3 M SiO_2 nanoparticles.

The best silicon deposits on graphite and silver substrates were compared. Silicon on graphite had a shorter deposition time (1 h vs 6 h), a smaller thickness (3.5 μm vs 7.0 μm) but still a higher photocurrent (1.71 mA/cm^2 vs 0.87 mA/cm^2) and smaller dark current. Thus the silicon deposits on graphite substrates were denser and of better quality and hence graphite is a more promising substrate for a silicon solid-state solar cell. The best photocurrent was 31% of that of our standard silicon wafer.

Acknowledgment

This work was funded by Dow Corning Corporation (UTA10-001176), the Global Climate and Energy Project (GCEP, Agreement No. 60853646-118146), and the Welch Foundation (F-0021)). Any opinions, findings, and conclusions or recommendations expressed in this publication are those of the author(s) and do not necessarily reflect the views of Stanford University, the Sponsors of the Global Climate and Energy Project, or others involved with the Global Climate and Energy Project.

Dr. Ji Zhao acknowledges the sponsorship from Chinese Postdoctoral Fellowship.

References

1. I. E. Agency, Technology Roadmap: Solar Thermal Electricity, in *Technology Roadmap*, M. v. d. Hoeven Editor, International Energy Agency (2014).
2. R. N. Andrews and S. J. Clarson, *Silicon*, **7**, 303 (2015).
3. U. S. D. O. Energy, SunShot Vision Study, in *SUNSHOT INITIATIVE*, R. Ramesh Editor, U.S. Department of Energy (2012).
4. ITRPV, International Technology Roadmap for Photovoltaic 2014 Results, in *International Technology Roadmap for Photovoltaic*, ITRPV, SEMI (2015).
5. J. M. Serra, *Energy Procedia*, **10**, 303 (2011).
6. M. J. Keevers, T. L. Young, U. Schubert, and M. A. Green, in *22nd European Photovoltaic Solar Energy Conference*, p. 1783 (2007).
7. S. Jeong, M. D. McGehee, and Y. Cui, *Nature communications*, **4** (2013).
8. B. Terheiden, T. Ballmann, R. Horbelt, Y. Schiele, S. Seren, J. Ebser, G. Hahn, V. Mertens, M. B. Koentopp, and M. Scherff, *physica status solidi (a)*, **212**, 13 (2015).
9. A. J. Bard and L. R. Faulkner, *Electrochemical methods: fundamentals and applications*, Wiley New York (2001).
10. F. Ullik, *SitzBer. Akad. Wiss. Wien*, **52**, 115 (1866).
11. R. Monnier and J. Giacometti, *Helv. Chim. Acta*, **47**, 345 (1964).
12. S. K. Cho, F.-R. F. Fan, and A. J. Bard, *Angew. Chem. Int. Ed.*, **51**, 12740 (2012).
13. J. Xu and G. M. Haarberg, *High Temperature Materials and Processes*, **32** (2013).
14. G. M. Rao, D. Elwell, and R. S. Feigelson, *J. Electrochem. Soc.*, **128**, 1708 (1981).
15. T. Nohira, K. Yasuda, and Y. Ito, *Nat. Mater.*, **2**, 397 (2003).
16. W. Xiao, X. Jin, Y. Deng, D. Wang, X. Hu, and G. Z. Chen, *Chemphyschem*, **7**, 1750 (2006).
17. K. Yasuda, T. Nohira, R. Hagiwara, and Y. Ogata, *Electrochim. Acta*, **53**, 106 (2007).
18. J. Zhao, S. Lu, L. Hu, and C. Li, *Journal of Energy Chemistry*, **22**, 819 (2013).
19. J. Zhao, J. Li, P. Ying, W. Zhang, L. Meng, and C. Li, *Chem Commun (Camb)*, **49**, 4477 (2013).
20. K. Maeda, K. Yasuda, T. Nohira, R. Hagiwara, and T. Homma, *Journal of the Electrochemical Society*, **162**, D444 (2015).
21. K. Yasuda, K. Maeda, T. Nohira, R. Hagiwara, and T. Homma, *Journal of The Electrochemical Society*, **163**, D95 (2015).
22. H. Ye, H. S. Park, V. A. Akhavan, B. W. Goodfellow, M. G. Panthani, B. A. Korgel, and A. J. Bard, *Journal of Physical Chemistry C*, **115**, 234 (2011).
23. C. Bird and A. Kuhn, *Chem. Soc. Rev.*, **10**, 49 (1981).
24. E. L. Warren, S. W. Boettcher, M. G. Walter, H. A. Atwater, and N. S. Lewis, *The Journal of Physical Chemistry C*, **115**, 594 (2011).
25. H. Van Dam and J. Ponjee, *J. Electrochem. Soc.*, **121**, 1555 (1974).
26. M. G. Walter, E. L. Warren, J. R. McKone, S. W. Boettcher, Q. Mi, E. A. Santori, and N. S. Lewis, *Chem. Rev.*, **110**, 6446 (2010).
27. S. K. Cho, A. J. Bard, and F.-R. F. Fan, Production of thin film solar grade silicon on metals by electrodeposition from silicon dioxide in a molten salt, in, WIPO Editor, Google Patents (2013).
28. N. S. Lewis, *Acc. Chem. Res.*, **23**, 176 (1990).
29. H. A. Audesirk, E. L. Warren, J. Ku, and N. S. Lewis, *ACS applied materials & interfaces*, **7**, 1396 (2015).
30. C. Seager, *J. Appl. Phys.*, **52**, 3960 (1981).
31. A. L. Bieber, L. Massot, M. Gibilaro, L. Cassayre, P. Taxil, and P. Chamelot, *Electrochim. Acta*, **62**, 282 (2012).
32. S. K. Cho, F.-R. F. Fan, and A. J. Bard, *Electrochim. Acta*, **65**, 57 (2012).
33. M. D. McCluskey and E. E. Haller, *Dopants and defects in semiconductors*, CRC Press (2012).
34. T. Wang, T. Ciszek, C. Schwerdtfeger, H. Moutinho, and R. Matson, *Solar energy materials and solar cells*, **41**, 19 (1996).
35. M. Schlesinger and M. Paunovic, *Modern electroplating*, John Wiley & Sons (2011).